Environmental Fluid Mechanics (2020) 20:433–457
https://doi.org/10.1007/s10652-019-09680-2

ORIGINAL ARTICLE

Modelling small ventilated corner baffles for box culvert barrel

Carlos Sailema[1] · Rubén Freire[1] · Hubert Chanson[1] · Gangfu Zhang[2]

Received: 10 January 2019 / Accepted: 20 March 2019 / Published online: 27 March 2019
© Springer Nature B.V. 2019

Abstract
During the last decades, concerns regarding the ecological impact of standard culverts have led to some design evolution. The installation of baffles along the culvert barrel yields smaller velocities and larger water depths in the barrel, potentially more suitable for upstream fish passage, albeit with a decrease in discharge capacity. Small triangular corner baffles were proposed to facilitate the upstream passage of small-body-mass fish, without compromising the discharge capacity of the culvert at design flow. Although fish benefited from low velocity regions for resting and sheltering, a small fraction of small-body-mass fish were observed to become disoriented by the adverse effect of flow reversal regions in the wake of plain baffles. This study presents the hydrodynamic testing of small ventilated triangular corner baffles for standard box culverts. The baffle ventilation was introduced to reduce the impact of negative wake behind the baffles. Two designs were tested: a baffle with three holes and a brush baffle. Detailed modelling in a near-full-scale culvert barrel showed that the ventilated corner baffles created a smaller negative wake region. A lesser negative velocity magnitude was observed behind the ventilated baffles, in comparison to plain baffles, for the same flow rate, baffle height and spacing. With ventilated corner baffles, the longitudinal distribution of low-velocity zone was more uniform, yielding a better longitudinal connectivity for upstream passage, compared to plain baffles. A comparison between various boundary treatments suggested however that the requirements for continuous, sizeable low positive velocity zone suitable to small-bodied fish might be better fulfilled with an asymmetrically roughened culvert barrel than with triangular baffles, even with ventilation.

Keywords Open channels · Corner baffles · Culvert barrel · Physical modelling · Computational fluid dynamics CFD · Low positive velocity zone LPVZ · Negative velocity zone NVZ

✉ Hubert Chanson
h.chanson@uq.edu.au
http://www.uq.edu.au/~e2hchans/

[1] School of Civil Engineering, The University of Queensland, Brisbane, QLD 4072, Australia

[2] WSP Australia, Brisbane, QLD 4000, Australia

1 Introduction

Longitudinal connectivity of streams constitutes a basic requirement for a healthy waterway with fauna and flora diversity. During the last decades, concerns regarding the ecological impact of road crossings have led to some evolution in design [1–3]. The impact in terms of fish passage may adversely affect both upstream and downstream catchments [4]. Common culvert fish passage barriers encompass perched outlet with excessive vertical drop at the culvert outlet, high velocities and turbulence in the barrel, debris accumulation at the culvert inlet, and standing waves in inlet and outlet [5–7]).

In response to ecological concerns, the installation of baffles along the culvert barrel invert have been promoted as some fish-friendly technique to decrease velocities and increase the water depth in the barrel, while offering resting zones, yielding potentially more adequate hydrodynamic conditions for fish passage [1, 8–10]. But baffles can reduce very significantly the culvert discharge capacity for a given afflux [6, 9]. Small triangular corner baffles were proposed as an alternative to create favourable conditions for upstream passage of small-body-mass fish, without compromising the discharge capacity of the culvert at design flow conditions [7] (Fig. 1a). Controlled tests with juvenile silver perch (*Bidyanus bidyanus*), weak swimming fish less than 10 cm long, indicated a preference for the fish to swim at the vicinity of baffles [11]. Fish benefited from low velocity regions for resting and sheltering, especially upstream of the small corner baffles. A number of small fish were observed to turn around and could get disoriented by the adverse effect of flow reversal regions in the wake of plain baffles [12] (Fig. 1b). Figure 1b illustrates one such example. Often the small-bodied fish escaped the recirculation region by swimming downstream and exited the culvert barrel channel outlet. A similar kind of observations was also reported behind horizontal square baffles [13]. Further the generation of large contiguous traversable low-velocity zones cannot be guaranteed for all flow rates with plain baffles, depending upon the relative longitudinal spacing [14].

This study presents the hydrodynamic modelling of ventilated triangular corner baffles for standard box culverts, developed to address the issue of negative wake behind the baffles. Two designs were developed: a baffle with three holes and a brush baffle. Their performances were tested under controlled flow conditions in a near-full-scale culvert barrel cell, in terms of the associated flow resistance, velocity distributions and size of low velocity zones (LVZs). The results were systematically compared to smooth channel and other boundary treatments (without baffles), previously tested with small-body-mass fish, i.e., juvenile silver perch (*Bidyanus bidyanus*) and adult Duboulay's rainbowfish (*Melanotaenia duboulayi*), in a similar culvert barrel flume. The present physical experiments were performed for a range of flow conditions corresponding to less-than-design discharges with a breadth of baffle configurations and spacings. Further numerical modelling was undertaken to examine the ventilation performance of the baffle with three holes.

2 Modelling and flow conditions

2.1 Baffle configurations

Several boundary treatments were tested in a 12 m long 0.5 m wide rectangular flume, corresponding to a near-full-scale culvert barrel cell beneath a 2-lane road embankment.

(A) Sketches of small corner baffle arrangements - From top left, clockwise direction: baffles on left corner only, baffles placed on left corner alternating two baffle sizes, baffles on both corners in an alternate arrangement, and baffles in both corners placed uniformly at same longitudinal location

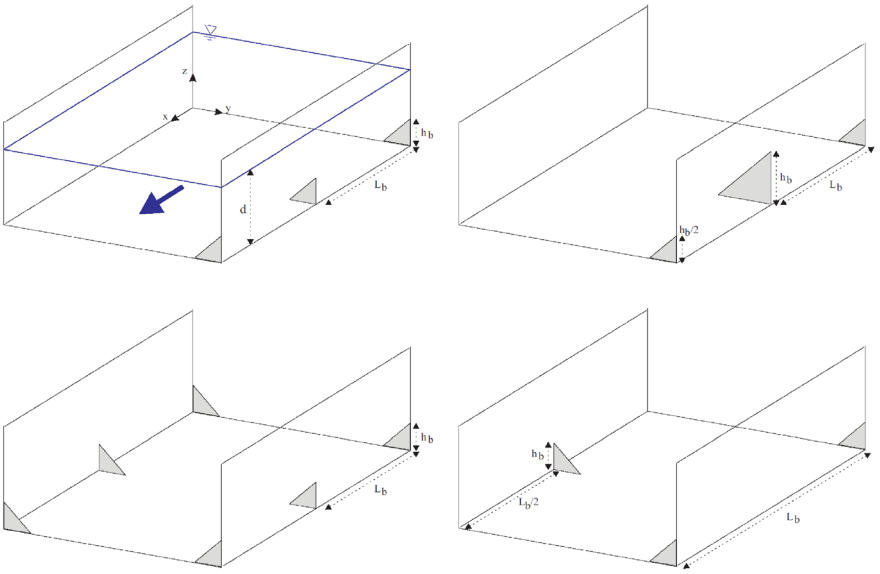

(B) High-speed video movie shots of a juvenile silver perch (*Bidyanus bidyanus*) trapped in the recirculation region downstream of a triangular corner baffle (h_b = 0.133 m) (Study: Cabonce et al. 2017, 2019) - The flow direction of the flow is from left to right (blue arrow) and the red arrow points to the baffle - Increasing time from left to right

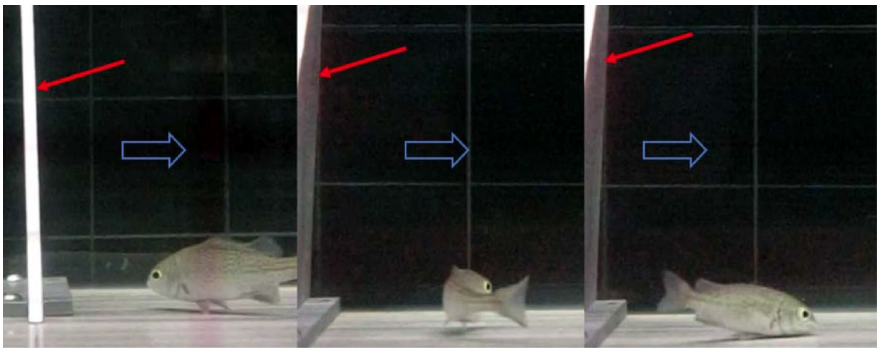

Fig. 1 Box culvert barrel with small triangular corner baffles

These configurations included: (a) smooth channel without baffle; (b) plain baffles (h_b = 0.067 m and 0.133 m); (c) brush baffles (h_b = 0.133 m); and (d) baffles with three holes (h_b = 0.133 m), with h_b being the baffle height (Fig. 1a). The smooth channel was used as reference. The plain baffles were isosceles triangular corner baffles, identical to the study of Cabonce et al. [11, 12], based upon preliminary tests by Chanson and Uys [7, 15]. Figure 2a shows a side-by-side comparison of the various types of baffles.

Two types of ventilated baffles were developed and tested. The brush baffles were isosceles triangles (h_b = 0.133 m) with a triangular permeable inner area which covered about 38% of

(A) Photograph of the various corner baffle types: plain baffle (h_b= 0.133 m), plain baffle (h_b= 0.133 m), baffle with three holes (h_b= 0.067 m), brush baffle (h_b= 0.133 m) from left to right

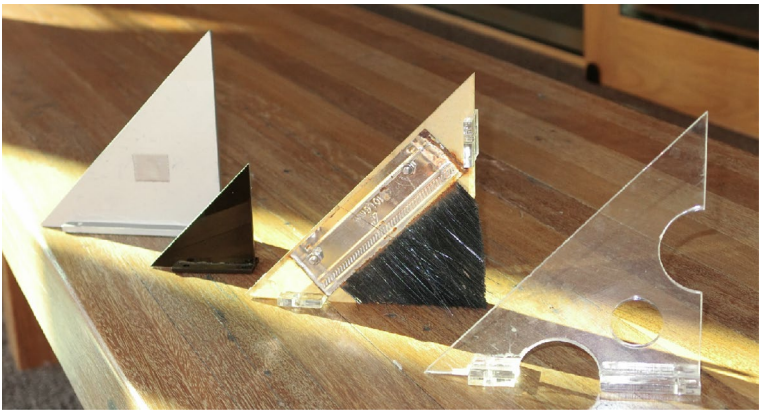

(B) Dimensioned drawings of brush baffle

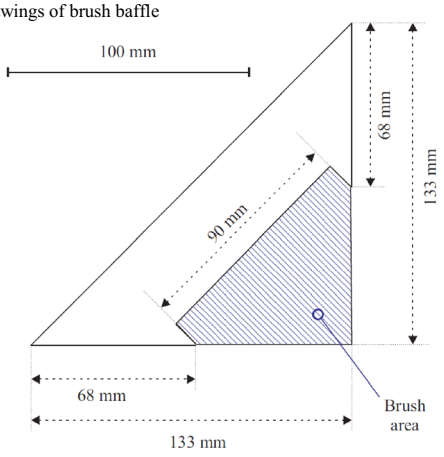

(C) Dimensioned drawings of baffle with three holes

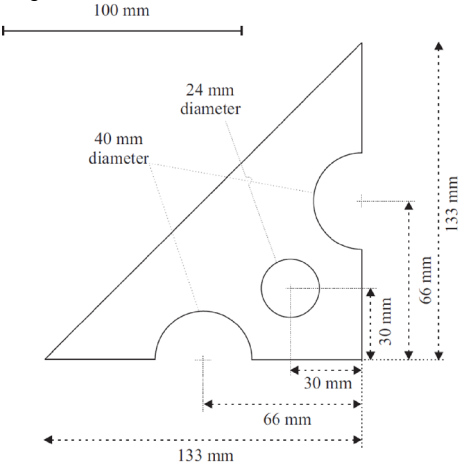

Fig. 2 Design of small ventilated corner baffles

the total baffle area (Fig. 2b). The permeable area was manufactured out of synthetic hollow BS-1519 Paint brush. The brush thickness was within 1.33–1.60 mm. The ventilated baffles with holes were isosceles triangles ($h_b = 0.133$ m) with two semi-circular openings (∅ 40 mm) along the boundaries and one circular opening (∅ 24 mm) (Fig. 2c). The cumulative opening represented 19% of the baffle projected area. For comparison, Cabonce et al. [12] tested baffles with a single ventilation hole (∅ 13 mm) corresponding to 1.5% of the baffle cross-section area. Figures 2b, c present dimensioned drawings of the new ventilated baffle designs.

For each type of baffle, several longitudinal arrangements were tested. They were (1) baffles on left corner only, (2) baffles on both corners in an alternate arrangement, and (3) baffles in both corners placed uniformly at same longitudinal locations. These three arrangements were configured with a constant baffle size and spacing for the whole flume. A fourth arrangement consisted of baffles placed on the left corner only, with alternating baffle sizes. (The alternance in baffle sizes was only undertaken for plain baffles.) Figure 1a shows the four baffle arrangements.

2.2 Physical modelling

The 12 m long 0.5 m wide laboratory flume was located in the AEB Hydraulics Laboratory of the University of Queensland and made of a smooth PVC bed and glass sidewalls. The test section presented similar dimensions to those of a real standard box culvert barrel cell, thus allowing a quasi 1:1 scale prototype-model testing. Water was supplied by a constant head tank into the flume intake, where baffles, flow straighteners and a three-dimensional convergent transition section allowed smooth inflow conditions into the 12 m long flume. The flume ended with a free overfall at the downstream end.

The water depth was measured using rail-mounted pointer gauges, with an accuracy of ±0.5 mm, except in the near wake of the corner baffles where the fluctuating water level was recorded through the glass sidewall. The water discharge was measured with an orifice meter designed based upon British Standards and calibrated on site, with an expected error of less than 2%.

A Dwyer® 166 Series Prandtl-Pitot tube was used to record velocity and pressure. The tube diameter was 3.18 mm with a hemispherical total pressure tapping at the tip (∅ 1.18 mm) and four static pressure holes (∅ 0.51 mm) equally spaced, located 25 mm behind the tip. The Prandtl-Pitot tube presented low sensitivity to misalignment up to ±15°. Calibration was not needed because of the ASHRAE tip design. Both total and piezometric pressures were measured with an inclined manometer opened to the atmosphere. The Prandtl-Pitot tube was calibrated as a Preston tube to measure the skin friction shear stress at the boundaries [11, 16]. The calibration curve matched closely an analytical solution of the Prandtl mixing length model in the wall region:

$$\tau'_o = \rho \times \kappa^2 \times \frac{V_b^2}{N^2} \quad (1)$$

where τ'_o is the local skin friction boundary shear stress, ρ is the fluid density, κ is the von Karman constant (κ = 0.4), N is the power law exponent, with N = 7 for smooth turbulent boundary layer flows [17], and V_b is the velocity measured by the Prandtl-Pitot tube positioned against the boundary. The Prandtl-Pitot tube was also tested to record negative velocities [11]:

$$V_x = -17.81 \times (-\Delta H)^{0.538} \quad (2)$$

where V_x is the velocity in m/s and ΔH is the difference between the total head and piezometric head in metres. Equation (2) was specifically developed for the Dwyer® 166 Prandtl-Pitot tube, although it is acknowledged that the results presented some scatter, because of the very small pressure difference between the total and piezometric head tappings.

Instantaneous velocity and velocity fluctuations were measured with acoustic Doppler velocimetry (ADV). Two systems were used: a Nortek™ Vectrino + equipped with a three-dimensional side-looking head, and a Sontek™ microADV equipped with a two-dimensional side-looking head. The ADV signal was recorded for 180 s at each data point, using sampling frequencies of 200 Hz and 50 Hz for the Vectrino + and microADV systems respectively. The ADV data were post-processed, by removing samples with average correlation below 60%, average signal to noise ration (SNR) below 5 dB and communication errors. In the near-wake of a baffle, a significant drop in average signal correlations was observed because of the high turbulent shear and velocity gradient across the ADV sampling volume [18–20], and samples with average correlation below 40% were removed. Further the phase-space thresholding technique was applied to remove spurious points [21, 22]. Finally data samples with less than 50% of good samples were discarded.

The vertical position of the Prandtl-Pitot tube and ADV units was controlled by fine traverse screw-drive mechanism and measured with a HAFCO™ digital micrometre with an error $\Delta z < \pm 0.01$ mm. Further details on the experimental facility and results were reported by Freire et al. [23].

2.3 Numerical CFD modelling

Three-dimensional numerical modelling was undertaken for the symmetric three-hole baffle configuration ($h_b = 0.133$ m, $L_b/h_b = 5$) in both corners placed uniformly at same longitudinal locations and one discharge ($Q = 0.0556$ m^3/s), using the commercial software ANSYS Fluent 19.2. The goal of this work was to reproduce the laboratory flow patterns and to gain insights into the detailed interactions between the flow and baffles, as well as the effect of baffle ventilation. The area of interest is around the reference baffle at $x_b = 8.16$ m, for which velocity and depth information are available, with x_b the longitudinal coordinate of the baffle location. The numerical domain measured 0.67 m × 0.50 m × 0.20 m (length × width × height) centered around the reference baffle. The domain height reflected the laboratory observations: $d = 0.199$–0.200 m, with d the water depth, and the longitudinal time statistics were assumed to be periodic with a wavelength of L_b, consistent with experimental observations. Smooth walls were adopted as the bottom and sidewall boundaries, and the free-surface was represented by a zero-shear wall. A mass flow equivalent to the laboratory flow conditions was imposed on the periodic boundaries and was maintained by the correct pressure gradient solved at each time step. The discretisation of the numerical domain was comprised of two sections of uniform structured hexahedral mesh (0.2 m long, 0.01 m × 0.01 m × 0.005 m cells) at the extremities of the domain joined by a section of unstructured hexahedral mesh (0.27 m long) around the baffle, totalling approximately 150,000 cells. A detached eddy simulation (DES) was selected to compensate for the relatively coarse mesh at the boundaries ($y^+ \approx 100$), with the Delayed DES (D-DES) option enabled to preserve the RANS model throughout the boundary layer. Herein y^+ is the dimensionless wall distance [24]. The numerical scheme automatically switched between RANS (realisable k–ε) and LES modes based on the distance to the nearest wall. The adopted numerical configuration represented a compromise between efficiency and

resolution, and was deemed appropriate for the present purpose, since the dominant large-scale motions induced by flow separation at baffle edges were directly resolved with LES.

Convergence criteria were defined for continuity, velocity and turbulence variables such that the solution advanced in time as the scaled residual for continuity decreased by five orders of magnitude (10^{-5}) and other variables by three orders of magnitude (10^{-3}). No mass imbalance was present as it was enforced by the periodic boundary condition. The simulation was allowed to run for approximately 25 s (~25 turnover times) before the time statistics were sampled for 30 s at 1000 Hz.

2.4 Experimental flow conditions

A total of 38 boundary configurations were tested. The reference experiments were performed with the smooth flume (no baffle). A series of experiments were conducted with plain baffles in the left corner only, for direct comparison with the study of Cabonce et al. [11]. Further experiments were undertaken with the three types of isosceles triangular corner baffles (plain, brush, holes). The baffles were fixed at the bottom corner(s). Several longitudinal baffle spacings were tested ($0.33\ \text{m} < L_b < 2.0\ \text{m}$) with two baffle heights ($h_b = 0.067$ m and 0.133 m). Table 1 summarises the experimental flow and boundary conditions.

Flow patterns and free-surface observations were performed for four discharges: $Q = 0.0261\ \text{m}^3/\text{s}$, $0.035\ \text{m}^3/\text{s}$, $0.0556\ \text{m}^3/\text{s}$ and $0.097\ \text{m}^3/\text{s}$ for all 38 boundary configurations (Table 1). The discharges corresponded to less-than-design flows for which a subcritical free-surface flow motion is observed in the culvert barrel for a mild slope. Detailed velocity measurements were conducted for one flow rate only with a smaller number of boundary configurations (Table 2). Informations of the velocity measurement experiments are reported in Table 2. The numerical CFD modelling was undertaken for one flow rate and the ventilated baffles with three holes (Table 3). In Tables 1 and 2, the present experimental conditions are compared to the works of Cabonce et al. [11, 12].

3 Basic flow patterns

3.1 Presentation

For all discharges, the free-surface was relatively smooth and flat in laboratory, with decreasing water depth with downstream distance (i.e., $\partial d/\partial x < 0$ with d the flow depth and x the longitudinal coordinate positive downstream). The flow was subcritical and gradually-varied throughout the entire flume for all flow rates within $0.0261\ \text{m}^3/\text{s} < Q < 0.097\ \text{m}^3/\text{s}$. The water depth became critical near the overfall at the flume's downstream end.

For all baffled configurations, the interaction between baffles and turbulent flow was evidenced visually. A localised reduction in water level next to the sidewall was observed immediately downstream of each baffle for all flow rates (Fig. 3). The water surface variations suggested localised turbulent dissipation linked to separation around the baffle edge and major flow redistribution in the wake of the baffles. Based upon ideal fluid theory, the localised dip downstream of a baffle may correspond to local fluid acceleration and pressure reduction [11]. For a given flow rate, the mean water depth was found to increase with increasing baffle size and decreasing baffle spacing, because of a larger effect of baffles on the flow resistance (next section). Similar flow patterns were observed for all plain baffles,

Table 1 Experimental study of small triangular corner baffles in culvert barrel flume

References	S_o	Q (m^3/s)	Baffle design	H_b (m)	L_b (m)	Baffle corner	Longitudinal pattern	Comments
Present study	0	0.0261, 0.035, 0.0556	–	–	–	–	–	Smooth channel
	0	0.0261, 0.035, 0.0556	Plain	0.067	0.33, 0.67, 1.0, 1.33, 1.67, 2.0	Left	–	Left corner only
		0.0261, 0.035, 0.0556		0.133		Left	–	
		0.0261, 0.035, 0.0556		0.067 and 0.133	0.33, 0.67, 1.0, 1.33, 1.67	Left	–	Alternating two baffle sizes
		0.0261, 0.035, 0.0556		0.067	0.33, 0.67, 1.0, 1.33, 1.67, 2.0	Both	Same location	Same longitudinal location
		0.0261, 0.035, 0.0556, 0.097		0.133		Both	Same location	
		0.0261, 0.035, 0.0556		0.067	0.67, 1.33, 2.0	Both	Alternate	Alternate arrangement
		0.0261, 0.035, 0.0556		0.133		Both	Alternate	
		0.0261, 0.035, 0.0556, 0.097	Brush	0.133	0.67	Both	Same location	Same longitudinal location
		0.0261, 0.035, 0.0556, 0.097	Holes	0.133	0.67	Both	Same location	Same longitudinal location
Cabonce et al. [11][1]	0	0.0261, 0.035, 0.0556	–	–	–	–	–	Smooth channel[1]
		0.0261, 0.035, 0.0556	Plain	0.033	0.33, 0.67, 1.0, 1.33, 1.67, 2.0	Left	–	Left corner only[1]
				0.067				
				0.133				
Cabonce et al. [12]	0	0.0261, 0.035, 0.0556	–	–	–	–	–	Smooth channel[1]
			Plain	0.133	0.67, 1.33, 1.67, 2.0	Left	–	Left corner only[1]
						Both	Same location	Same longitudinal location
			Hole[2]	0.133	0.67, 1.33, 1.67, 2.0	Left	–	Left corner only
						Both	Same location	Same longitudinal location

h_b triangular baffle height, L_b baffle spacing, S_o bed slope

[1]Channel equipped with upstream and downstream screens; [2]∅13 mm hole

Table 2 Detailed velocity measurements in culvert barrel flume equipped with small triangular corner baffles - Physical modelling

References	S_o	Q (m^3/s)	Baffle design	h_b (m)	L_b (m)	Baffle corner	Comments
Present study	0	0.0556	Plain	0.133	0.67	Both	Same longitudinal location
			Brush	0.133	0.67	Both	Same longitudinal location
			Holes	0.133	0.67	Both	Same longitudinal location
Cabonce et al. [11, 16][1]	0	0.0261, 0.0556	–	–	–	–	Smooth channel
		0.0261, 0.0556	Plain	0.067	0.67	Left	Left corner only
		0.0556		0.133	0.67		
		0.0261, 0.0556		0.133	1.33		
Cabonce et al. [12]	0	0.0556	Hole[2]	0.133	0.67	Left	Left corner only

h_b triangular baffle height, L_b baffle spacing, S_o bed slope

[1]Channel equipped with upstream and downstream screens; [2]∅13 mm hole

Table 3 Computational fluid dynamic configuration for culvert barrel channel equipped with triangular corner baffles with three holes

Item	Configuration	Notes
Channel geometry	$0.67 \times 0.50 \times 0.20$ m^3	Length × width × height
Baffle	$h_b = 0.133$ m, L = 0.67 m, baffles with 3 holes	Placed uniformly in both corners at same longitudinal location
Mesh	Structured and unstructured hexahedral	152,041 cells; structured near boundaries and unstructured around baffle
Model	D-DES	Default coefficients
Top boundary	Zero shear wall	–
Side boundaries	No-slip wall	–
Bottom boundary	No-slip wall	–
Inlet type	Periodic	Mass flow rate 55.6 kg/s
Solution	SIMPLE/2nd order time and space	–

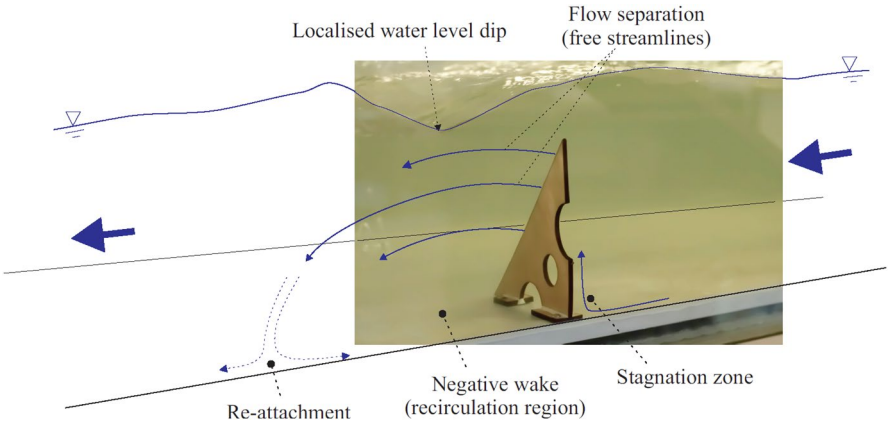

Fig. 3 Flow field around a triangular corner baffle—flow conditions: Q = 0.0556 m^3/s, h_b = 0.133 m, L_b = 0.67 m, ventilated baffles with three holes in both corners placed uniformly at same longitudinal location, flow direction from right to left

comparable to the observations of Cabonce et al. [11]. Key flow features in terms of fish passage were the stagnation region immediately upstream of each baffle and the negative wake immediately downstream (Fig. 3). The former was shown to have beneficial impact on upstream passage of small-body-mass fish, while the latter had adverse impacts [11, 12]. With the particular arrangement of baffles in both corners at alternate locations, the flow visualisation showed a meandering pattern around the triangular baffles. The resulting flow field yielded non-continuous low velocity zones (LVZs) in the flume corners, which would not be conducive to upstream fish migration [14].

Flow visualisation was further conducted using dye injection. For all plain baffle arrangements, sizes and spacings, the recirculation zone length was observed to be

about twice the baffle height. This finding is comparable, albeit slightly smaller than the observations of Cabonce et al. [11], but might reflect different lighting conditions between laboratory halls. With plain baffles in both corners in an alternate arrangement, the lower flow motion experienced a marked meandering motion between the baffles. The negative wake appeared to be slightly shorter, i.e., about 1.5 times the baffle height, likely as a result of the meandering streamlines in the lower water column. With the ventilated baffle arrangements (Table 1), a recirculation zone was also identified behind each baffle. However the dye seeped for a shorter time in the stagnation region, upstream of the ventilated baffles, as some dye passed through the holes and brush. The recirculation length behind each ventilated baffle appeared to be comparable to, albeit shorter than that with plain baffles. It was seen to be about 1.5 times the baffle height for both brush baffles and baffles with holes: that is, 25% shorter than with plain baffles.

3.2 Flow resistance

The flow resistance of triangular baffled flumes was tested in the physical model and compared to smooth channel results for discharges: $0.0261\ m^3/s < Q < 0.097\ m^3/s$ and 38 boundary configurations. The spatially-averaged boundary shear stress was deduced from the measured free-surface profiles and total energy slope, i.e. friction slope S_f, with an uncertainty of about 5%. The friction slope S_f is related to the Darcy-Weisbach friction factor f by:

$$S_f = f \times \frac{V_{mean}^2}{2 \times g \times D_H} \tag{3}$$

where V_{mean} is the cross-sectional averaged velocity, g is the gravity acceleration and D_H is the equivalent pipe diameter [25, 26]. The present results in terms of the Darcy-Weisbach friction factor f are reported in Fig. 4. The friction factor is basically a dimensionless spatially-averaged boundary shear stress [25, 27]:

$$f = \frac{\tau_o}{\frac{1}{8} \times \rho \times V_{mean}^2} \tag{4}$$

with τ_o the spatially-averaged boundary shear stress.

The main results are presented in Fig. 4, and the full data set is reported in Freire et al. [23]. Figure 4a–c show the Darcy–Weisbach friction factor data to be a function of the relative baffle height h_b/D_H. The smooth flume data compared favourably with previous data in similar smooth flumes, as well as with the Karman–Nikuradse formula:

$$\frac{1}{\sqrt{f_s}} = 2.0 \times \log_{10}\left(Re \times \sqrt{f_s}\right) - 0.8 \tag{5}$$

where f_s is the friction factor for smooth turbulent flows and Re is the Reynolds number [17, 24]. In the presence of corner baffles, the flow resistance increased with increasing relative baffle height h_b/D_H, as seen in Fig. 4. With plain corner baffles, the friction factor data followed closely the data of Cabonce et al. [12] for the same relative baffle height (Fig. 4, Blue lines). Further the Darcy–Weibach friction factor decreased with increasing Reynolds number for all baffle configurations (Fig. 4d). A typical example is presented in Fig. 4d, for baffles on both corners uniformaly located with $h_b = 0.133$ m and $L_b = 0.67$ m. The results

(A, Left) Triangular baffles in left corner only

(B, Right) Triangular baffles in both corners placed uniformly at same longitudinal location

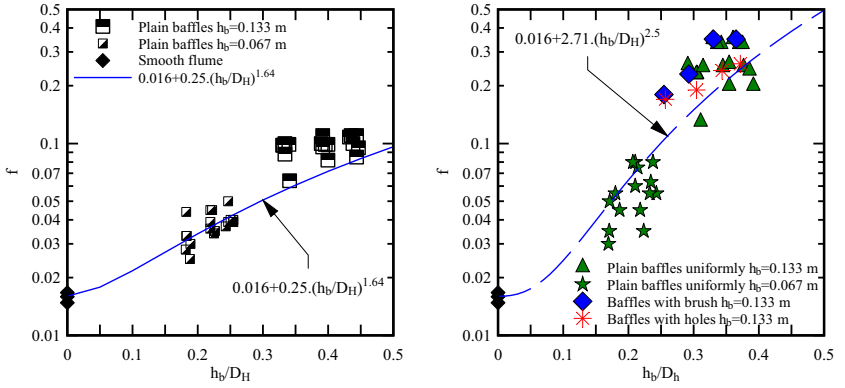

(C, Left) Triangular baffles in both corners in an alternate arrangement

(D, Right) Darcy-Weisbach friction factor as a function of the Reynolds number for h_b = 0.133 m, L_b = 0.67 m, baffles in both corners placed uniformly at same longitudinal location - Comparison between smooth flume data (no baffles), plain baffle, brush baffle and baffle with holes configurations:

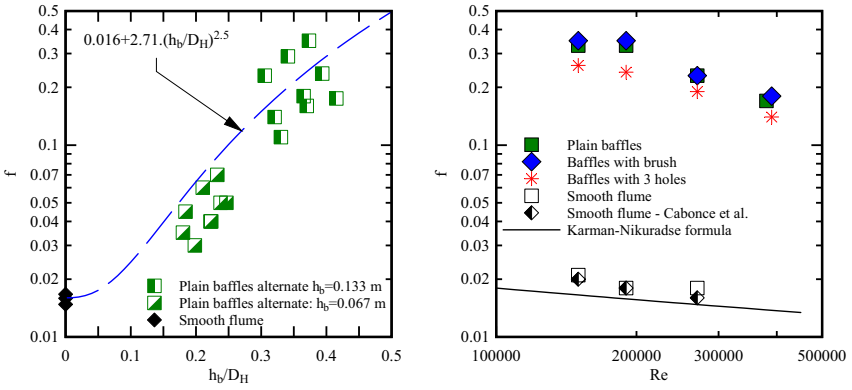

Fig. 4 Darcy–Weisbach friction factor as a function of the relative baffle height to baffle h_b/D_H—comparison with smooth flume data ($h_b = 0$) and data of Cabonce et al. [12] (blue curves)

imply a trend for which the presence of small triangular baffles would be expected to have a moderate effect on the flow resistance at larger discharges, i.e., larger Reynolds numbers, corresponding to culvert design flows.

4 Velocity field

4.1 Presentation

Detailed velocity measurements were conducted in the experimental flume with baffles in both corners uniformly placed with a relative longitudinal spacing $L_b/h_b = 5$ for one flow rate $Q = 0.0556$ m^3/s (Table 2). The focus of the physical experiments was a comparison of the velocity field between plain baffles and ventilated baffles. Four cross sections ($x - x_b = 0.03$ m, 0.167 m, 0.335 m, 0.5 m) were selected, with the reference baffle located at $x = x_b = 8.16$ m. These corresponded to a relative distance X between two baffles: $X = 0.05$, 0.25. 0.5 and 0.75, with $X = (x - x_b)/L_b$ and L_b the longitudinal baffle spacing.

Since the baffles were uniformly placed on both corners at the same location, the velocity field was basically symmetrical about the channel centreline at each cross section. The central region of the channel was characterised by a high velocity zone with $V_x > V_{mean}$, where V_x is the longitudinal velocity component and V_{mean} is the cross-sectional averaged velocity. Low velocity zones (LVZs) were observed next to the sidewall boundaries. Negative velocities were recorded in the near-wake of the baffles where recirculation patterns were observed using dye injection. The negative velocities were the largest at the cross section $x - x_b = 0.167$ m ($X = 0.25$) for both plain and ventilated baffles. The ventilated baffle configurations showed significantly-less-pronounced negative velocities in comparison to the plain baffle configuration, as initially reported by Cabonce et al. [12] with lesser ventilation. For plain baffles, the largest recirculation velocity was $V_x = -0.95$ m/s, comparable to the observations of Cabonce et al. [11]. With ventilated baffles, the largest recirculation velocity was -0.65 m/s and -0.5 m/s for brush baffles and baffles with holes respectively. With ventilated baffles, the cavity ventilation replenished the negative wake, yielding a shorter negative wake with less intense recirculation velocities. Figure 5 presents the contour plots of time-averaged longitudinal velocity V_x for the plain baffle configuration, while Fig. 6 presents typical results for ventilated baffles. In Figs. 5 and 6, the solid black lines correspond to the edges of the corner baffles.

The presence of corner baffles yielded a complicated flow motion with secondary currents of Prandtl's second kind. Next to the bottom corners, the flow was retarded, and some flow motion was generated at right angle to the longitudinal current: i.e., some secondary currents [28, 29]. Further the secondary currents interact with curved streamlines induced by the corner baffle edges. With both plain and ventilated baffles, the cross-sectional maximum velocity was recorded on the channel centreline close to the free-surface. At all other transverse locations, the local maximum velocity was observed below the free-surface. For both plain and ventilated baffles, the dimensionless ratio V_{max}/V_{mean} was distributed in a symmetric manner with respect to the flume centreline ($y/B = 0.5$) [23].

Velocity fluctuations were recorded using the acoustic Doppler velocimeter ADV at a limited number of transverse locations. Figure 7 shows typical contours of longitudinal velocity fluctuations downstream of brush baffles. In Fig. 7, the solid black lines correspond to the edges of the corner baffles. For both plain and ventilated baffles, large velocity fluctuations were observed in the separation region downstream of the edges of the triangular baffles. The separation lines are sketched in Fig. 3 and corresponded to a thin region with very-high velocity gradient and turbulent shear. In the present study, the velocity fluctuation data were symmetrical about the flume centreline, and consistent with the symmetrical baffle configurations. Similar findings were obtained with the transverse velocity fluctuations (data not shown).

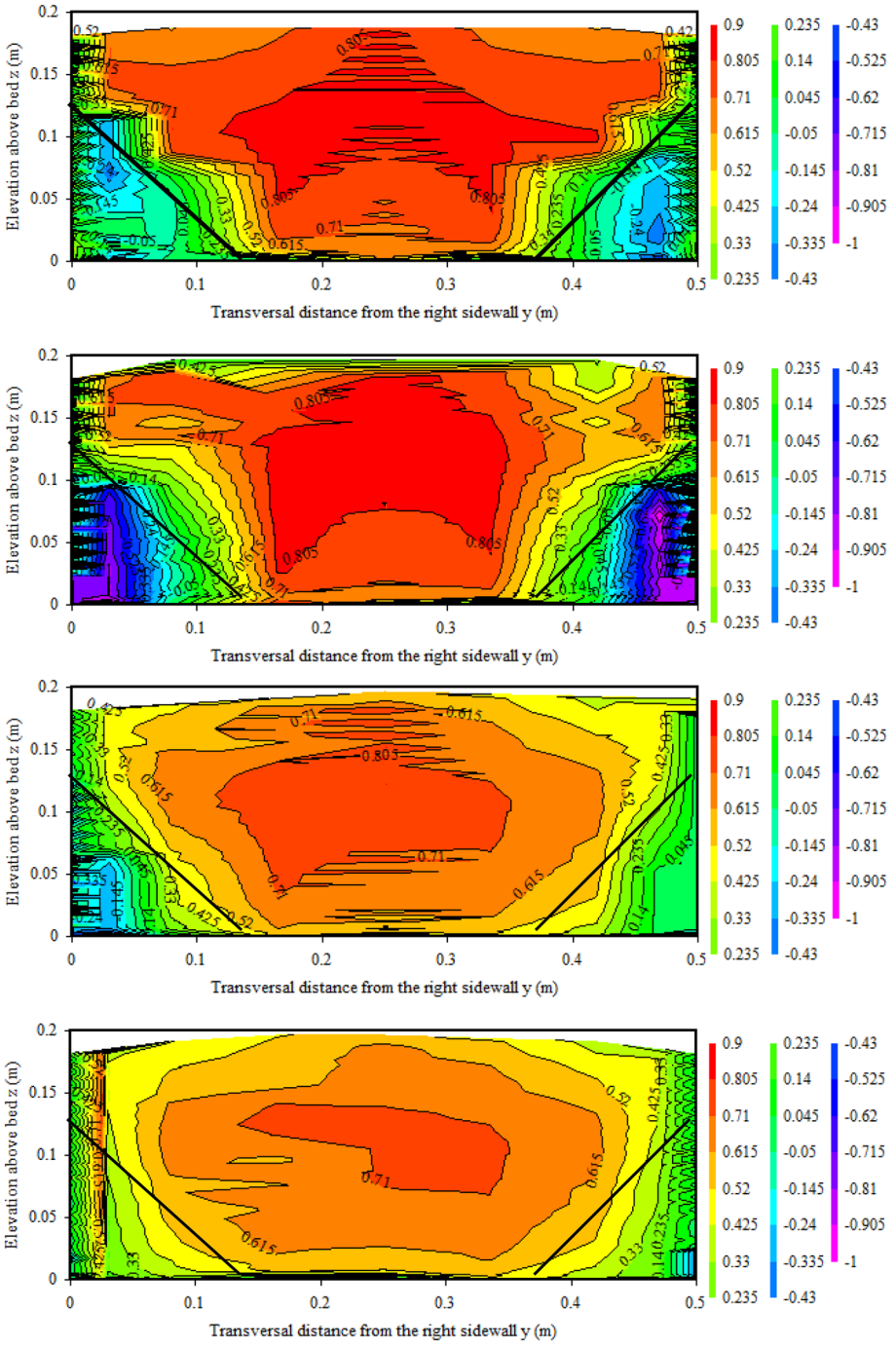

Fig. 5 Contour plots of time-averaged longitudinal velocity V_x (in m/s) for plain baffles—physical modelling: Q = 0.0556 m^3/s, d = 0.197 m, h_b = 0.133 m, L_b = 0.67 m, x_b = 8.16 m, plain baffles in both corners placed uniformly at same longitudinal location—from top to bottom: x = 8.19 m, 8.3275 m, 8.495 m and 8.66 m (X = 0.05, 0.25, 0.50 and 0.75)

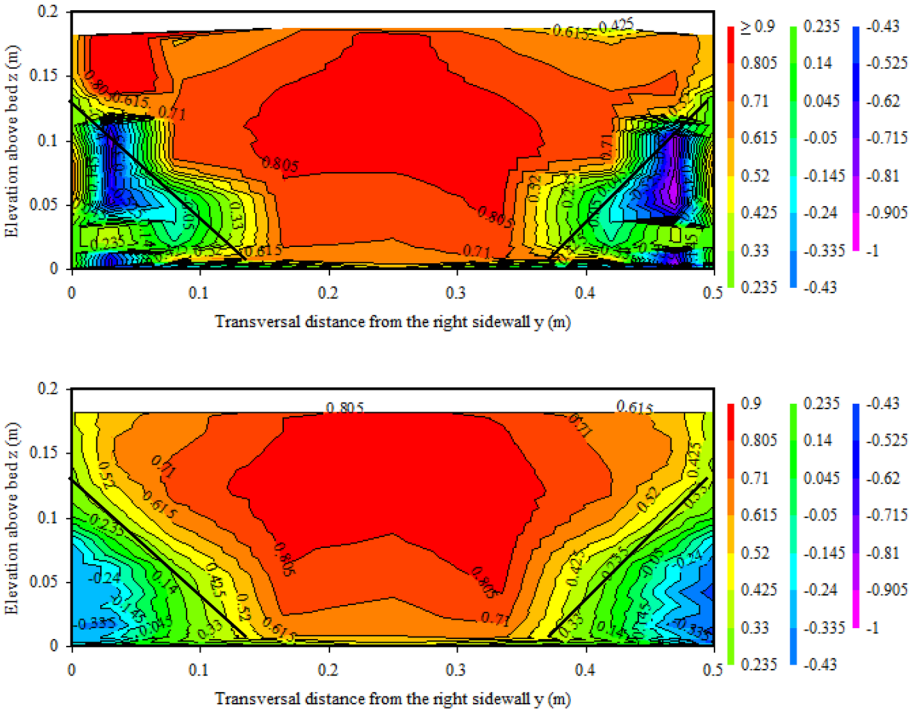

Fig. 6 Contour plots of time-averaged longitudinal velocity V_x (in m/s) for baffles with three holes—physical modelling: Q = 0.0556 m^3/s, d = 0.200 m, h_b = 0.133 m, L_b = 0.67 m, x_b = 8.16 m, baffles with holes in both corners placed uniformly at same longitudinal location—from top to bottom: x = 8.19 m and 8.3275 m (X = 0.05 and 0.25)

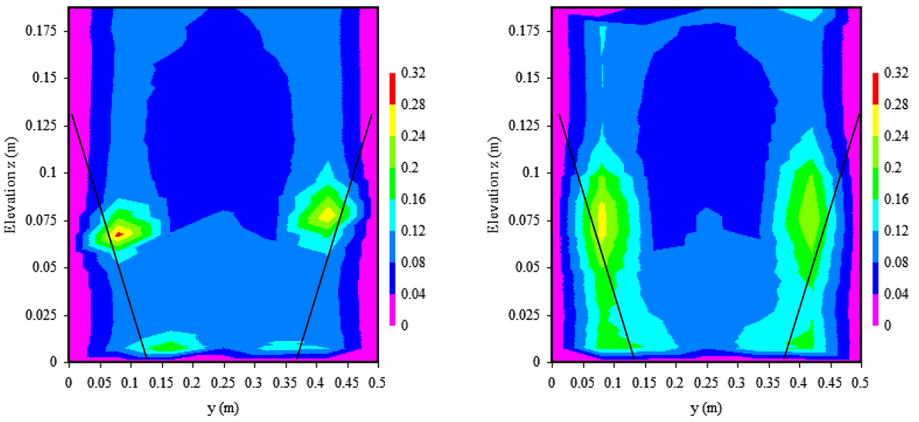

Fig. 7 Contour plots of longitudinal velocity fluctuations v'_x (m/s) with brush baffles—physical modelling: Q = 0.0556 m^3/s, d = 0.199 m, h_b = 0.133 m, L_b = 0.67 m, x_b = 8.16 m, brush baffles in both corners placed uniformly at same longitudinal location—from left to right: x = 8.19 m & 8.3275 m (X = 0.05 and 0.25)

4.2 Discussion

The numerically-simulated time-averaged longitudinal velocity contours are presented in Fig. 8 for the three-hole baffles. The global flow patterns was qualitatively comparable to the physical observations, i.e., with a high velocity core at the centre of the channel and low velocity regions in the corners and behind the baffles. Additional features included the high velocity jets discharging through the baffle openings, and large velocity gradients behind the baffle's long edge due to separation. The peak recirculating velocity (−0.15 m/s) was approximately one-third of the present laboratory observations (−0.5 m/s). A further inspection of the physical experimental data (Fig. 6) revealed dips in the velocity contours induced by secondary currents that were either less pronounced or not exhibited in the numerical results, e.g., at the bottom of the channel and near toes of the baffles, likely in consequence of the isotropic wall model (k–ε). Overall the results showed that the ventilating jets quickly dissipated into the surrounding fluid and a globally positive flow was restored at approximately halfway between two baffles.

The flow field responses to the ventilated baffles are further illustrated in Fig. 9, which were volume-rendered to highlight low velocity zones, below preselected thresholds: i.e.,

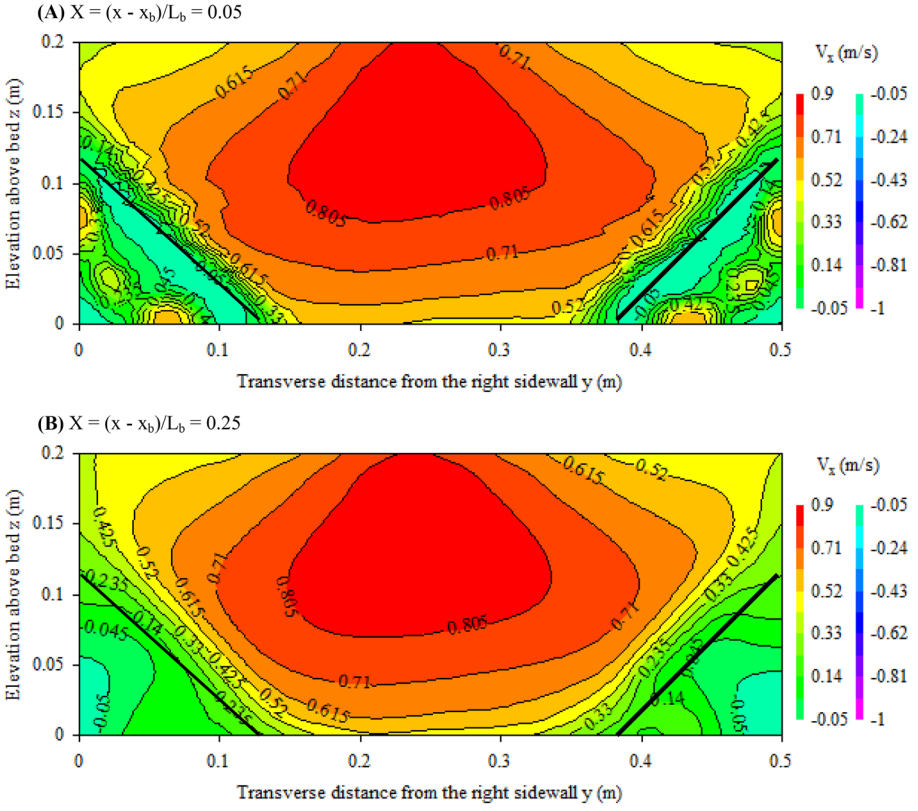

Fig. 8 Time-averaged streamwise velocity contours (V_x) for baffles with three holes—numerical CFD modelling: Q = 0.0556 m^3/s, d = 0.2 m, h_b = 0.133 m, L_b = 0.67 m, x_b = 8.16 m. **a** X = (x − x_b)/L_b = 0.05. **b** X = (x − x_b)/L_b = 0.25

$V_x < 0$, $V_x < 0.25 \times V_{mean}$, and $V_x < 0.5 \times V_{mean}$, based upon the numerical results. Low velocities are rendered in darker shades, and velocities larger than the thresholds are not represented in Fig. 9. The recirculation zone, i.e., the negative velocity zone (NVZ), appears to be of approximately twice the baffle size and actively interacted with the ventilating jets in the immediate wake of the baffle. The turbulent jets carved through the surrounding low velocity fluid and split the recirculation zone in two, i.e., one at the corner and one past the baffle edge. The recirculation zone past the baffle long edge was initially highly turbulent and dissipated quickly, while mixing with the high velocity jets. The corner recirculation grew and diminished in size over a significant length and finally dissipates by approximately halfway between adjacent baffles.

The low-velocity zones (LVZs) developed in the corner region immediately upstream and downstream of the baffle, due to stagnating and streamline separations respectively (Fig. 3). The upstream LVZ is favoured by small-bodied fish as a rest area [12], but appears to diminish in size compared to plain baffles due to flow ventilation. The downstream LVZ is largest in the immediate wake of the baffle, and interacts with the ventilating jets over a region of comparable dimensions to the blockage. The LVZs reduced to negligible size around $(x–x_b)/L_b = 0.75$ before redeveloping towards the next downstream baffle.

5 Boundary shear stress

The boundary shear stress was recorded with the Prandtl-Pitot tube, acting as a Preston tube, along the channel bed and channel sidewalls in the laboratory culvert barrel channel. Results are reported in Fig. 10, as contour maps of the skin friction on the channel boundaries. In Fig. 10, the flow direction is from left to right, the solid lines indicate the bottom corners and the dotted lines correspond to the locations of the baffles.

The boundary shear stress data showed some symmetrical distribution of the skin friction about the flume centreline. With plain baffles, the skin friction shear stress was consistently larger than that behind the ventilated baffles, for the same discharge, baffle height and spacing (Fig. 10). The result was likely linked to the ventilation of the wake and the modification of the flow field behind the baffle. In the baffled channels, the data showed that the skin friction boundary shear stress was significantly less than the total boundary shear stress: i.e., $(\tau_o)_{skin}/\tau_o < 1$, as previously reported for a channel configuration with plain triangular baffles in the left corner only [11].

The skin friction shear stress data were integrated along the wetted surface area, yielding the spatial-averaged skin friction boundary shear stress over one baffle longitudinal spacing L_b:

$$\overline{(\tau_o)_{skin}} = \frac{1}{L_b \times P_w} \times \int_{L_b} \int_{P_w} (\tau_o)_{skin} \times dy \times dx \tag{6}$$

where P_w is the wetted perimeter and y'' is the transverse coordinate following the wetted perimeter, with $y'' = 0$ at the bottom right corner (Fig. 10a). Depending upon the baffle configuration, the ratio of mean skin friction resistance to total flow resistance $\overline{(\tau_o)_{skin}} / \tau_o$ ranged from 0.05 to 0.08 (Table 4). Such results inferred that the flow resistance was primarily form drag, for the small triangular baffled culvert barrel. The full results are reported in Table 4. The data in terms of spatial-averaged skin friction were similar to the

Fig. 9 Volume rendering of computed low-velocity zones (LVZs) behind baffles with three holes - Numerical CFD modelling ($Q = 0.0556$ m^3/s); Darker shading correspond to lower velocity, Flow direction from bottom right to top left ▶

finding of Cabonce et al. [11], although that study measured the bed shear stress data only, excluding sidewalls.

6 Discussion

6.1 Low velocity zones

Considering a fish negotiating a culvert barrel, the fish minimises its energy expenditure by swimming in low velocity zones (LVZs) during upstream passage [30, 31]. Several studies showed that fish, especially small-bodied fish, preferentially swim next to the culvert walls and in the corner regions [11–13, 16, 32–35]. The relative size of low velocity zone (LVZ) may be defined as a fraction of the wetted flow area, typically next to the wetted perimeter (Fig. 10a). The present velocity measurement data were analysed to quantify the size of low-velocity-zone (LVZ) in terms of the percentage of cross sectional flow area for which the time averaged longitudinal velocity V_x was less than V_{mean}, $0.75 \times V_{mean}$, $0.5 \times V_{mean}$ and zero (i.e. negative velocity area). Full results are presented in Freire et al. [23].

For both plain and ventilated baffles, the longitudinal distribution of LVZ was not uniform. The LVZ was larger immediately downstream of the baffle, i.e., $X \leq 0.25$, where X is the relative distance between two baffles. Further downstream the size of LVZ was substantially reduced. With plain baffles, 5–31% of the cross sectional area experienced velocities less than $0.5 \times V_{mean}$. These percentages decreased for ventilated baffles for the same baffle height and longitudinal spacing: namely 5–22% of the cross sectional velocity field was less than $0.5 \times V_{mean}$. Such a reduction of low velocity regions was expected because to the baffle ventilation.

Fish swimming experiments showed that the negative wake immediately downstream of triangular baffles could disorient small-body-mass fish [11, 12]. The size of the negative velocity zone (NVZ) should be minimised and it is thus a relevant design parameter. For plain baffles, a large NVZ was identified covering most area in the wake of the baffles, i.e., $X \leq 0.25$. Negative velocities up to − .99 m/s were recorded and the NVZ covered up to 13% of the cross section area. With ventilated baffles, the NVZ represented less than 7% and 9% of the flow cross-section area for brush baffles and baffles with holes.

The experimental findings of the present study may be compared to those by Wang et al. [7] and Cabonce et al. [11, 12] with smooth flume, rough wall and bed channel, and flume with triangular baffles on the left corner. The LVZ size was 5–10% area for smooth channel conditions, 17% for rough wall and bed, 14–26% for plain triangular baffles ($h_b = 0.133$ m, $L_b = 0.67$ m) placed on one corner only, and 16–28% for triangular baffles with Ø13 mm hole ($h_b = 0.133$ m, $L_b = 0.67$ m) placed on one corner only.

6.2 On fish passage and longitudinal connectivity of low positive velocity zone

Low-velocity zones suitable for upstream passage of small-bodied fish should fulfil:

$$0 < V_x < U_{fish} \tag{7}$$

(A) $V_x < 0$ - Negative Velocity Zone (NVZ)

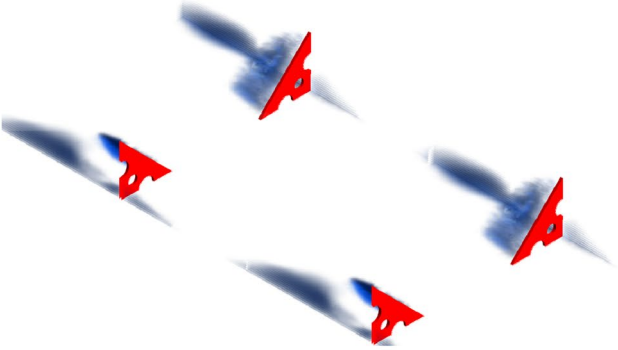

(B) $V_x < 0.25 \times V_{mean}$

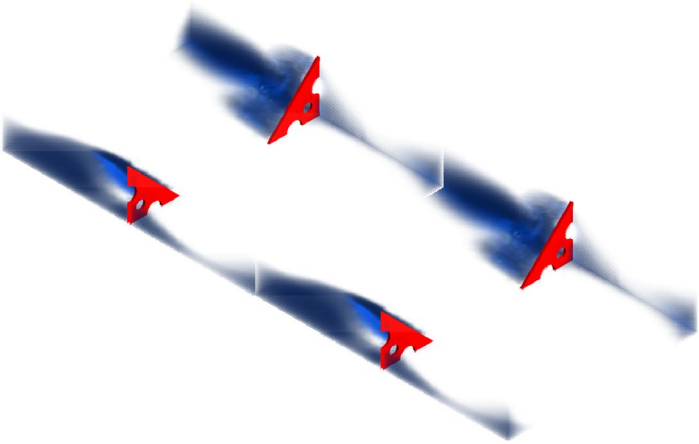

(C) $V_x < 0.5 \times V_{mean}$

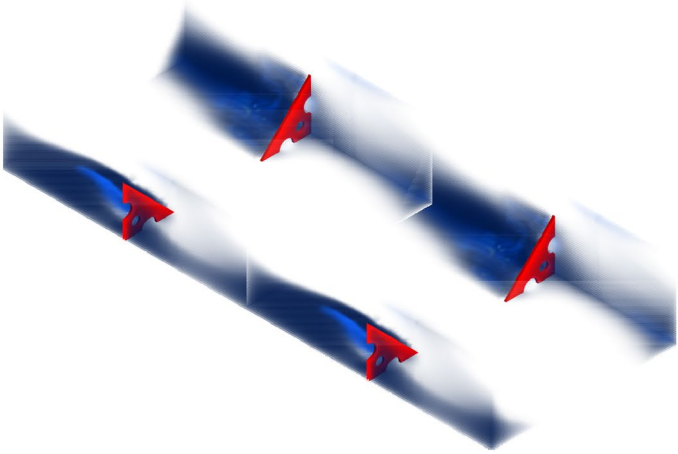

Fig. 10 Contour plots of boundary shear stress $(\tau_o)_{skin}$ (Units: Pascals) in triangular baffle channels—flow direction from left to right, Physical modelling, $Q = 0.0556$ m^3/s, $h_b = 0.133$ m, $L_b = 0.67$ m, $x_b = 8.16$ m, baffles in both corners placed uniformly at same longitudinal location—Horizontal solid black lines are channel corners and vertical dotted lines are the baffle location ▶

where V_x is the local time-averaged longitudinal velocity component and U_{fish} is a characteristic fish swimming speed ([11], [36]). Fish navigability in a culvert barrel also depends on the connectivity between low velocity zones (LVZs), in addition to their total relative size. In plain terms, long contiguous reaches of low positive velocity zone (LPVZ) which meet certain velocity criteria, e.g., $0 < V_x < U_{fish}$, are naturally more traversable than multiple, separate patches of LVZs [14].

Altogether, the present configurations appear to have limited effectiveness for upstream fish passage as a result of: (a) significant streamwise variation in LVZ sizes difficult to guide fish along a constant path; (b) ventilation strategy with limited penetration depth which fails to reduce/eliminate negative velocity zones (NVZs) beyond the immediate wake of the baffle; and (c) strong vortex shedding dynamics at a timescale that could affect the consistency of passage windows for fish, i.e. LVZs fluctuate in time and could be of similar frequencies to response times of certain species.

The performances of several types of flume boundary conditions were compared in terms of the relative size of low positive velocity zone where $0 < V_x < 0.5 \times V_{mean}$ (LPVZ), and its longitudinal distribution. Figure 11 presents a comparison in longitudinal connectivity of low positive velocity zone, from detailed hydrodynamic data obtained in 12 m long 0.5 m wide horizontal flumes for the same discharge. In Fig. 11, the present physical data are compared to earlier experimental data from smooth flume, and rough wall and bed channel (without baffles) [7, 11]. The results showed marked differences between the different boundary treatments (Fig. 11). In the smooth and rough flumes, the flow resistance was regularly distributed and flow separation was negligible. Continuous low-positive-velocity zones were provided next to the channel boundaries and in the corner regions, with a large LPVZ area fraction in the rough wall and bed flume (Fig. 11). With triangular baffles, flow separation took place at each baffle edge, followed by a wake region. Immediately downstream of the baffles, the size of LPVZ was comparable to that in the rough wall and bed flume, but only for a short distance. A lack of longitudinal LPVZ interconnection was clearly documented, as evidenced in Fig. 11.

7 Conclusion

A hydraulic engineering study of small corner baffles was conducted in a near-full-scale culvert barrel flume. The corner baffles were designed to create a sizeable low-velocity zone (LVZ) suitable for the upstream passage of small-body-mass fish in standard box culverts for less-than-design discharges, while having minimum impact on the culvert discharge capacity at design flows. Recent investigations showed that small-body-mass fish species could be disoriented by the negative wake immediately downstream of plain corner baffles [11, 12]. Ventilated corner baffles were developed herein to reduce the size of the negative velocity zones (NVZs): brush baffles with 38% pervious area and three-holes baffles with 19% openings. The complete hydrodynamic characteristics were systematically investigated in the present study, although their impact on fish behaviour and passage was not tested.

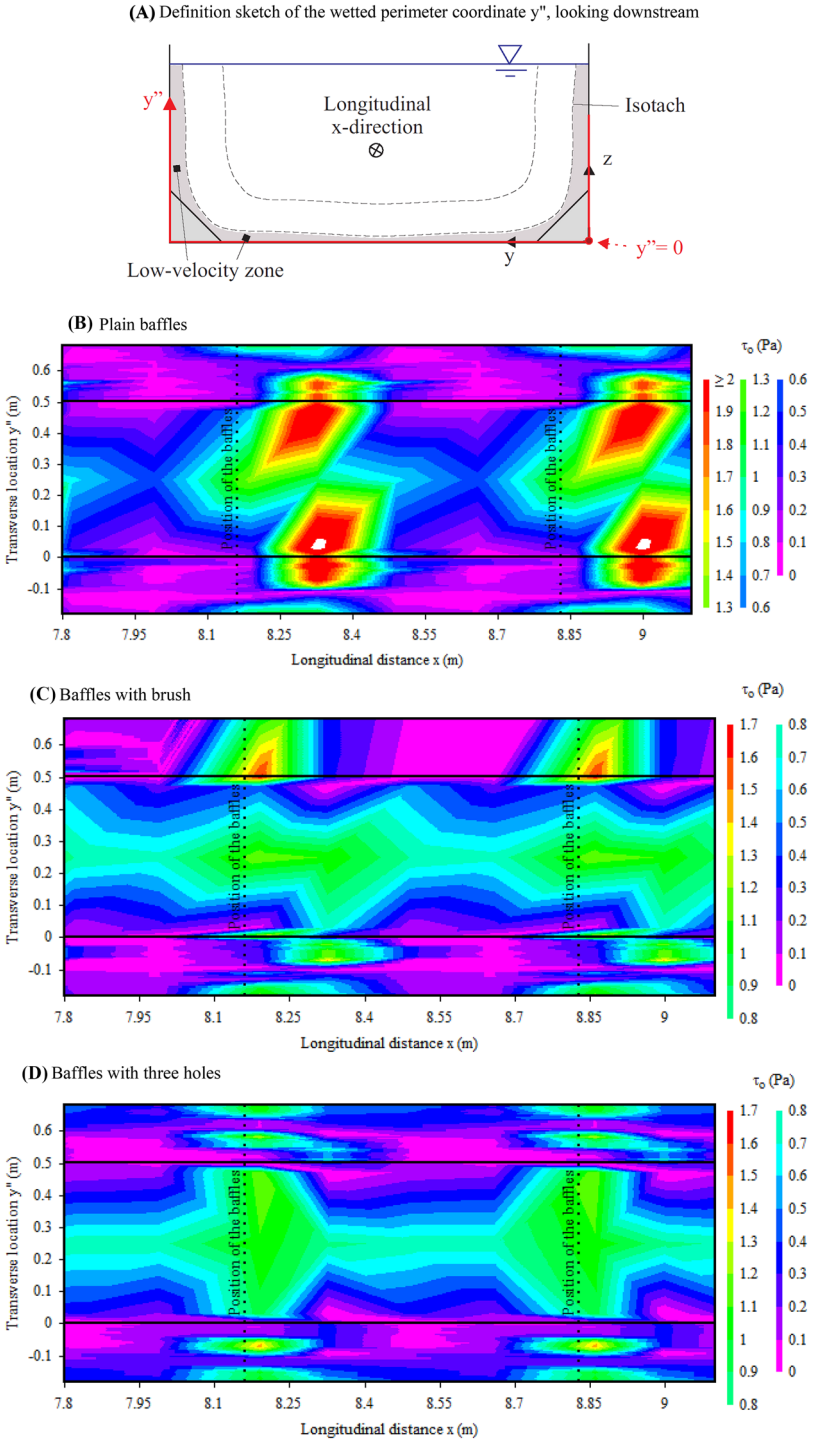
(A) Definition sketch of the wetted perimeter coordinate y", looking downstream
y"
Longitudinal
x-direction
Isotach
z
y
y"= 0
Low-velocity zone
(B) Plain baffles
(C) Baffles with brush
(D) Baffles with three holes
Transverse location y" (m)
Longitudinal distance x (m)
Position of the baffles
τo (Pa)

Table 4 Spatial-averaged skin friction boundary shear stress in triangular baffle channels (x ≈ 8 m)—physical modelling data—comparison with the experimental data of Cabonce et al. [11]

Boundary configuration	Baffle corner	Baffle height, h_b (m)	Baffle spacing, L_b (m)	Q (m^3/s)	d (m)	V_{mean} (m/s)	f	$\overline{(\tau_o)_{skin}}$ (Pa)	$\overline{f_{skin}}$	$\overline{f_{skin}}$ /f
Present study										
Plain baffles	Both	0.133	0.67	0.0556	0.20	0.542	0.23	0.776	0.0193	0.084
Brush baffles	Both	0.133	0.67		0.199	0.55	0.23	0.366	0.0092	0.048
Baffles with holes	Both	0.133	0.67		0.197	0.564	0.19	0.501	0.0146	0.064
Cabonce et al. [11]										
Smooth channel	–	N/A	N/A	0.0261	0.096	0.544	0.016	–	–	–
	–	N/A	N/A	0.0556	0.162	0.686	0.0145	–	–	–
Plain baffles	Left	0.067	0.66	0.0261	0.1	0.431	0.0325	0.436 (*)	0.0188 (*)	0.58 (*)
	Left	0.067	0.66	0.0556	0.1625	0.684	0.0365	0.599 (*)	0.0102 (*)	0.28 (*)
	Left	0.133	0.66	0.0556	0.166	0.643	0.059	0.660 (*)	0.0128 (*)	0.22 (*)
	Left	0.133	1.33	0.0556	0.172	0.647	0.053	0.674 (*)	0.0129 (*)	0.24 (*)

f: dimensionless total boundary shear stress; $\overline{f_{skin}}$: dimensionless skin friction boundary shear stress; V_{mean}: cross-section average velocity; $\overline{(\tau_o)_{skin}}$: spatial-averaged skin friction boundary shear stress; spatial averaging calculated over a baffle spacing L_b; (*): bed shear stress data only, excluding sidewall

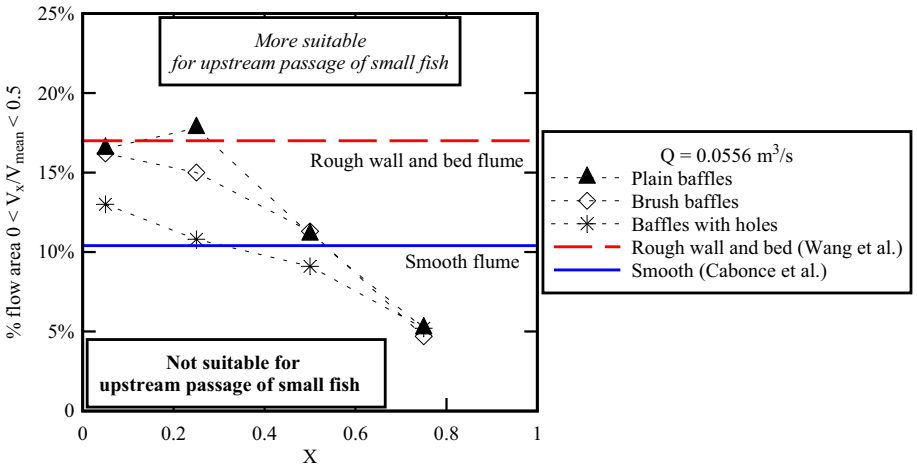

Fig. 11 Longitudinal variation of fractions of low positive velocity zone (LPVZ), i.e. $0 < V_x < 0.5 \times V_{mean}$, for plain baffles, brush baffles and baffles with holes - Physical modelling: $Q = 0.0556$ m^3/s, $B = 0.5$ m, $h_b = 0.133$ m, $L_b = 0.67$ m, $x_b = 8.16$ m, $X = 0.05$, 0.25, 0.5 & 0.75, baffles in both corners placed uniformly at same longitudinal location - Comparison with smooth and rough flume data (no baffles) ([11], [7]) for the same water discharge $Q = 0.0556$ m^3/s, barrel flume width ($B = 0.5$ m) and bed slope ($S_o = 0$)

The hydrodynamic performances of small corner baffle configurations were recorded thoroughly, with a focus on a systematic comparison between plain and ventilated baffles. The baffle ventilation reduced the size of the downstream wake, and consequently the negative local velocity magnitudes. The flow passing through the baffle holes and brush tended to break up the large coherent structures in the wake into smaller less organised eddies. The ventilated baffles induced a shorter recirculation zone with smaller negative recirculation, as evidenced by dye injection observations and detailed velocity measurements. Flow resistance results showed that the presence of triangular baffles would be expected to have a moderate effect on the culvert performances at large discharges corresponding to design flows. For both plain and ventilated baffles, large turbulence levels were observed in the separation region downstream the edges of the triangular corner baffles.

The concept of low positive velocity zone (LPVZ) and negative velocity zone (NVZ) was introduced as important indicators for the upstream culvert passage of small-body-mass fish. The LPVZ size and their longitudinal distribution showed marked differences between different channel boundary treatments. With triangular baffles, sizeable LPVZs were provided only for a short distance immediately downstream of the baffle, and a lack of longitudinal LPVZ interconnection was clearly documented. In smooth and rough flumes (no baffles), the boundary shear stress was regularly distributed with negligible flow separation and NVZ, delivering continuous low-positive-velocity zones (LPVZs) next to the channel boundaries and in the corner region. Present measurements suggested that the requirements for continuous, sizeable low positive velocity zone (e.g., $0 < V_x < 0.5 \times V_{mean}$) suitable to small-body-mass fish might be better fulfilled with an asymmetrically roughened culvert barrel than with triangular baffles, even with ventilation.

Acknowledgements The authors thank Professor Blake Tullis (Utah State University, USA) for his valuable comments. They thank also the reviewers for their constructive comments. The authors acknowledge the technical assistance of Youkai Li, Jason Van Der Gevel and Stewart Matthews (The University

of Queensland). The financial support through the Australian Research Council (Grant LP140100225) is acknowledged.

References

1. Chorda J, Larinier M, Font S (1995) Le Franchissement par les Poissons Migrateurs des Buses et Autres Ouvrages de Rétablissement des Ecoulements Naturels lors des Aménagements Routiers et Autoroutes. Etude Expérimentale. *Rapport HYDRE no159—GHAAPPE no 95-03*, Groupe d'Hydraulique Appliquée aux Aménagements Piscicoles et à la Protection de l'Environnement, Service d'Etudes Techniques des Routes et Autoroutes, Toulouse, France (in French)
2. Hotchkiss RH, Frei CM (2007) Design for fish passage at roadway-stream crossings: synthesis report. In: Publication No. FHWA-HIF-07-033, Federal High Way Administration, US Department of Transportation
3. Warren ML Jr, Pardew MG (1998) Road crossings as barriers to small-stream fish movement. Trans Am Fish Soc 127:637–644
4. Briggs AS, Galarowicz TL (2013) Fish passage through culverts in central Michigan warmwater streams. North Am J Fish Manag 33:652–664
5. Behlke CE, Kane DL, McLeen RF, Travis MT (1991) Fundamentals of culvert design for passage of weak-swimming fish. In: Report FHW A-AK-RD-90-10, Department of Transportation and Public Facilities, State of Alaska, Fairbanks, USA, 178 pages
6. Olsen A, Tullis B (2013) Laboratory study of fish passage and discharge capacity in slip-lined, baffled culverts. J Hydraul Eng ASCE 139(4):424–432
7. Wang H, Uys W, Chanson H (2018) Alternative Mitigation measures for fish passage in standard box culverts: physical modelling. J Hydro Environ Res IAHR 19:214–223. https://doi.org/10.1016/j.jher.2017.03.001
8. Cahoon JE, McMahon T, Solcz A, Blank M, Stein O (2007) Fish passage in Montana culverts: Phase II—passage goals. In: Report FHWA/MT-07-010/8181. Montana Department of Transportation and US Department of Transportation, Federal Highway Administration, 61 pages
9. Larinier M (2002) Fish passage through culverts, rock weirs and estuarine obstructions. Bull Franç Pêche Piscic 364(18):119–134
10. Khodier MA, Tullis BP (2014) Fish passage behavior for severe hydraulic conditions in baffled culverts. J Hydraul Eng ASCE 140(3):322–327. https://doi.org/10.1061/(ASCE)HY.1943-7900.0000831
11. Cabonce J, Fernando R, Wang H, Chanson H (2019) Using small triangular baffles to facilitate upstream fish passage in standard box culverts. Environ Fluid Mech 19(1):157–179. https://doi.org/10.1007/s10652-018-9604-x
12. Cabonce J, Wang H, Chanson H (2018) Ventilated corner baffles to assist upstream passage of small-bodied fish in box culverts. J Irrig Drain Eng ASCE. https://doi.org/10.1061/(ASCE)IR.1943-4774.0001329
13. Duguay J, Foster B, Lacey J, Castro-Santos T (2018) Sediment infilling benefits rainbow trout passage in a baffled channel. Ecol Eng 125:38–49. https://doi.org/10.1016/j.ecoleng.2018.10.003
14. Zhang G, Chanson H (2018) Three-dimensional numerical simulations of smooth, asymmetrically roughened, and baffled culverts for upstream passage of small-bodied fish. River Res Appl 34(8):957–964. https://doi.org/10.1002/rra.3346
15. Chanson H, Uys W (2016) Baffle designs to facilitate fish passage in box culverts: a preliminary study. In: Crookston B, Tullis B (eds) Proceedings of 6th IAHR international symposium on hydraulic structures, Hydraulic Structures and Water System Management, 27–30 June, Portland OR, USA, pp 295–304. https://doi.org/10.15142/t300628160828
16. Cabonce J, Fernando R, Wang H, Chanson H (2017) Using triangular baffles to facilitate upstream fish passage in box culverts: physical modelling. In: Hydraulic Model Report No. CH107/17, School of Civil Engineering, The University of Queensland, Brisbane, Australia. ISBN: 978-1-74272-186-6
17. Chanson H (2014) Applied hydrodynamics: an introduction. CRC Press, Taylor & Francis Group, Leiden. ISBN: 978-1-138-00093-3
18. Chanson H (2008) Acoustic doppler velocimetry (ADV) in the field and in laboratory: practical experiences. In: Larrarte F, Chanson H (eds.) Proceedings of the international meeting on measurements and hydraulics of sewers IMMHS'08. Summer School GEMCEA/LCPC, 19–21 Aug. 2008, Bouguenais. Hydraulic Model Report No. CH70/08, Division of Civil Engineering, The University of Queensland, Brisbane, Australia, Dec., pp 49–66

19. Chanson H, Trevethan M, Koch C (2007) Turbulence measurements with acoustic doppler velocimeters. J Hydraul Eng ASCE 133(11):1283–1286. https://doi.org/10.1061/(ASCE)0733-9429(2005)131:12(1062)
20. Martin V, Fisher TSR, Millar RG, Quick MC (2002) ADV data analysis for turbulent flows: low correlation problem. In: Proceedings of conference on hydraulic measurements and experimental methods, ASCE-EWRI & IAHR, Estes Park, USA (CD-ROM)
21. Goring DG, Nikora VI (2002) Despiking acoustic doppler velocimeter data. J Hydraul Eng ASCE 128(1):117–126 **Discussion: Vol. 129, No. 6, pp. 484-489**
22. Wahl TL (2003) Despiking acoustic doppler velocimeter data. J Hyd Eng, ASCE 129(6):484–487
23. Freire R, Sailema C, Chanson H (2018) On ventilated corner baffles for box culvert barrel: a physical investigation. In: Hydraulic Model Report No. CH112/18, School of Civil Engineering, The University of Queensland, Brisbane, Australia. ISBN: 978-1-74272-222-1
24. Schlichting H (1979) Boundary layer theory, 7th edn. McGraw-Hill, New York
25. Chanson H (2004) The hydraulics of open channel flow: an introduction, 2nd edn. Butterworth-Heinemann, Oxford. ISBN 978-0-7506-5978-9
26. Henderson FM (1966) Open channel flow. MacMillan Company, New York
27. Liggett JA (1994) Fluid mechanics. McGraw-Hill, New York
28. Gerard R (1978) Secondary flow in noncircular conduits. J Hydraul Div ASCE 104(HY5):755–773
29. Perkins HJ (1970) The formation of streamwise vorticity in turbulent flow. J Fluid Mech 44(4):721–740
30. Wang H, Chanson H (2018) Modelling upstream fish passage in standard box culverts: interplay between turbulence, fish kinematics, and energetics. River Res Appl 34(3):244–252. https://doi.org/10.1002/rra.3245
31. Wang H, Chanson H (2018) On upstream fish passage in standard box culverts: interactions between fish and turbulence. J Ecohydraul IAHR 3(1):18–29. https://doi.org/10.1080/24705357.2018.1440183
32. Blank MD (2008) Advanced studies of fish passage through culverts: 1-D and 3-D hydraulic modelling of velocity, fish energy expenditure, and a new barrier assessment method. Ph.D. thesis, Montana State University, Department of Civil Engineering, 231 pages
33. Gardner A (2006) Fish passage through road culverts. Master of Science thesis, North Carolina State University, USA
34. Jensen KM (2014) Velocity reduction factors in near boundary flow and the effect on fish passage through culverts. Master of Science thesis, Brigham Young University, USA
35. Wang H, Chanson H, Kern P, Franklin C (2016) Culvert hydrodynamics to enhance upstream fish passage: fish response to turbulence. In: Ivey G, Zhou T, Jones N, Draper S (eds) Proceedings of 20th Australasian fluid mechanics conference, Australasian Fluid Mechanics Society, Perth WA, Australia, 5–8 December, Paper 682, 4 pages
36. Chanson H, Leng X (2018) On the development of hydraulic engineering guidelines for fish-friendly standard box culverts, with a focus on small-body fish. Civil Engineering Research Bulletin No. 25, School of Civil Engineering, The University of Queensland, Brisbane, Australia

Publisher's Note Springer Nature remains neutral with regard to jurisdictional claims in published maps and institutional affiliations.